



---

## **A Comprehensive Investigation of Polymer-Grafted Carbon Nanoparticle Characterization and Synthesis**

**Dr Manisha Saxena, Department of Chemistry  
Government PG college, Dholpur (Rajasthan)**

### **ABSTRACT**

Due to their distinctive characteristics and possible uses, polymer-grafted carbon nanoparticles (PGCNs) have attracted a lot of attention in a number of sectors. In order to give readers a better grasp of the structure, characteristics, and synthesis techniques of PGCNs, this extensive inquiry focuses on their characterization and synthesis. Different analytical approaches are used to clarify the morphological, structural, and chemical characteristics of PGCNs. The size, form, and surface morphology of the nanoparticles are investigated using transmission electron microscopy (TEM) and scanning electron microscopy (SEM). The grafted polymers' chemical bonds and functional groups are identified using FTIR (Fourier-transform infrared spectroscopy) and Raman spectroscopy. The degree of graphitization and crystalline structure of the carbon core are examined using X-ray diffraction (XRD) examination. The synthesis of PGCNs is a multi-step process involving the preparation of carbon nanoparticles and subsequent grafting of polymer chains onto their surfaces. Different synthesis techniques such as chemical vapor deposition (CVD), sol-gel method, and emulsion polymerization are explored, each offering unique advantages in terms of control over particle size, polymer composition, and grafting density. The effects of various reaction parameters, such as temperature, time, precursor concentration, and initiator type, on the synthesis process and resulting PGCN properties are systematically investigated.

### **INTRODUCTION**

Polymer-grafted carbon nanoparticles (PGCNs) have garnered a lot of interest across a variety of industries due to their unique properties and potential applications. This thorough investigation concentrates on the characterization and synthesis of PGCNs to provide readers with a better understanding of their structure, properties, and synthesis methods. To further understand the morphological, structural, and chemical properties of PGCNs, various analytical techniques are



applied. Transmission electron microscopy (TEM) and scanning electron microscopy (SEM) are used to examine the nanoparticles' size, shape, and surface morphology. FTIR (Fourier-transform infrared spectroscopy) and Raman spectroscopy are used to determine the chemical bonds and functional groups of the grafted polymers. X-ray diffraction (XRD) analysis is used to determine how much of the carbon core is graphitized and what kind of crystalline structure it has. The objective of this comprehensive investigation is to delve into the characterization techniques employed to elucidate the morphological, structural, and chemical properties of PGCNs. Additionally, the synthesis methods used to prepare PGCNs with controlled composition, size, and grafting density will be explored.

Characterization of PGCNs involves a combination of analytical techniques to probe their morphology, structure, and chemical composition. Transmission electron microscopy (TEM) and scanning electron microscopy (SEM) provide detailed information about the size, shape, and surface morphology of the carbon nanoparticles. These techniques enable the examination of the core-shell structure, particle dispersion, and the presence of any agglomerations. Fourier-transform infrared spectroscopy (FTIR) and Raman spectroscopy are employed to identify the chemical bonds and functional groups present in the grafted polymers, offering insights into the nature of the polymer chains and their interaction with the carbon core. X-ray diffraction (XRD) analysis is used to investigate the crystalline structure and degree of graphitization of the carbon nanoparticles (Hwang, G. L. et al, 2004).

The synthesis of PGCNs involves a multi-step process, starting with the preparation of carbon nanoparticles and subsequent grafting of polymer chains onto their surfaces. Various synthesis techniques have been employed, each offering unique advantages in terms of control over particle size, composition, and grafting density. Common methods include chemical vapor deposition (CVD), sol-gel processes, and emulsion polymerization. These techniques allow for the precise tuning of parameters such as temperature, reaction time, precursor concentration, and initiator type, which influence the resulting PGCN properties. Understanding the effects of these parameters on the synthesis process is crucial for achieving desired nanoparticle characteristics and tailoring their properties for specific applications.

The potential applications of PGCNs span a wide range of fields. In the electronics sector,



PGCNs can be utilized in conductive inks, flexible electronic devices, and sensors, where their enhanced electrical conductivity and mechanical properties are advantageous. In energy storage, PGCNs show promise as electrode materials for supercapacitors and batteries, offering high surface area, improved charge storage, and stability. Biomedical applications include drug delivery systems, bioimaging agents, and tissue engineering scaffolds, where PGCNs can provide targeted drug release, imaging capabilities, and mechanical support. Additionally, PGCNs can be employed in environmental applications such as pollutant removal, water purification, and catalysis, leveraging their adsorption capacity and catalytic properties. This investigation aims to comprehensively explore the characterization and synthesis of PGCNs. By examining their morphological, structural, and chemical properties, a deeper understanding of PGCNs can be obtained, facilitating their optimization for specific applications. Moreover, the investigation seeks to highlight the potential of PGCNs in various fields and inspire further research and development in this exciting area of materials science (Baskaran, D. et al, 2004).

### **Material and Methods**

**Chemicals and materials:** Materials used in the present work are: Polystyrene from Sigma Aldrich, commercial, Acrylonitrile from Merck, Germany. Carbon nanotubes and dimethyl formamide (DMF) from BDH Limited Poole England. Ferrous ammonium sulphate (FAS) a grade from Fluka-Garantic used and. Chloroform and ethanol from Scharlau.

**Techniques:** The irradiation procedure for grafting polystyrene with acrylonitrile using activated carbon as a modifying agent was conducted using gamma irradiation. The experimental setup involved placing the polystyrene and acrylonitrile mixture in Pyrex tubes along with chloroform as a solvent and FAS as a catalyst. The irradiation process was carried out under ambient air conditions. To initiate the grafting reaction, the gamma irradiation was performed at a rate of 1.1 Mrad h<sup>-1</sup> using a Co Canadian type gamma cell 220. This irradiation method ensured the penetration of high-energy gamma rays into the reaction mixture, enabling the initiation of polymerization and grafting reactions.

**FTIR Measurement:** The FTIR spectra of the polymer were recorded using an IRAFFINITY-1 (8400) Fourier Transform spectrophotometer manufactured by SHIMAZAU, Japan. The measurements were performed at room temperature. The characterization of the polymer was

carried out using the KBr disc method. In the KBr disc method, the sample was first dried and ground together with KBr powder until they formed a well-mixed powdered mixture. The resulting powder was then pressed at a pressure of 8 tons for 1 minute to produce a compact disc. This disc contained the sample and KBr, which served as a matrix for the FTIR analysis. The FTIR measurements were conducted over a wave number range of 4000-400  $\text{cm}^{-1}$ . This range allowed for the analysis of various functional groups and chemical bonds present in the polymer. By scanning the sample within this range, the FTIR spectrophotometer generated a spectrum that provided information about the molecular vibrations and structural characteristics of the polymer.

### ANALYSIS OFFTIRSPECTRA:

Figure frames normal wide digestion for H-supported hydroxyl social occasions of carboxylic (OH), phenolic (OH), or boozier (OH) packs at 3422  $\text{cm}^{-1}$  in the FTIR spectra of GO. The broadness disappears in GOT, and a somewhat extraordinary sign in a comparative reach is seen, which can be credited to the (N-H) extending vibration. Curiously, on account of GOT, the sign at 1728  $\text{cm}^{-1}$  relates to the carboxyl gathering extending (C=O).

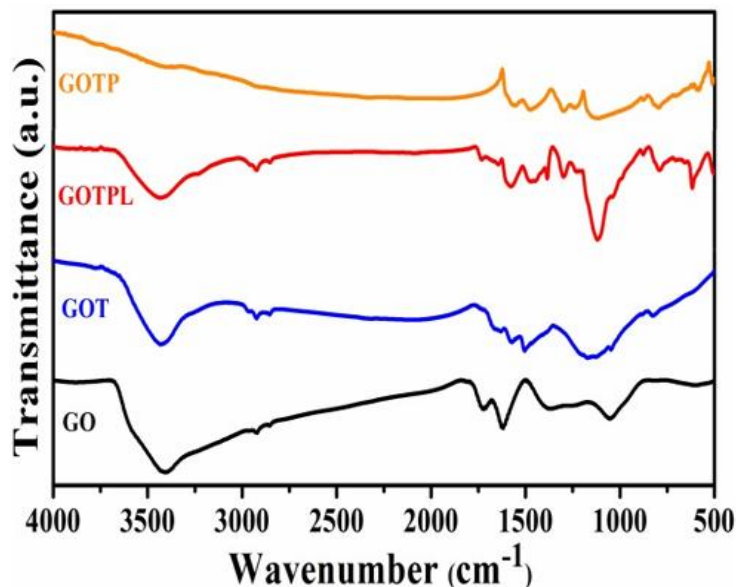


Figure 1: FTIR spectra for GO, GOT, GOTPL, GOTP samples respectively.



At the point when APQD moieties are connected to the (- COOH) gatherings of GO sheets, the sign at 1660  $\text{cm}^{-1}$  disappears and another top at 1660  $\text{cm}^{-1}$  creates, demonstrating the anilide carbonyl gathering. Any remaining generally low energy extending and bowing methods of GO and APQD are addressed by the wide sign in the district of 1300  $\text{cm}^{-1}$  to 1014  $\text{cm}^{-1}$ . A generally extensive sign at 3422  $\text{cm}^{-1}$  by virtue of GOTPL, which could show broadly H-supported amine social events of PANI ties due to doping with L-HCSA. The sign at 2921  $\text{cm}^{-1}$  is serious areas of strength for less, (C-H) reaching out of PANI chains' benzenoid or quinonoid rings. The sign at 1736  $\text{cm}^{-1}$  most likely addresses the carbonyl expanding vibration of CSA(-) moieties, which is missing in GOTP. At 3422  $\text{cm}^{-1}$  and 3422  $\text{cm}^{-1}$ , separately, the (C=C) broadening vibrations for quinonoid and benzenoid rings are seen. The presence of CSA(-) anions outlined by doping PANI chains with HCSA is confirmed by maintenances in the extent of 1060  $\text{cm}^{-1}$  to 660  $\text{cm}^{-1}$  by virtue of GOTPL. The gatherings at 1298  $\text{cm}^{-1}$ , 1231  $\text{cm}^{-1}$ , and 1123  $\text{cm}^{-1}$ , independently, show (C-N) assistant fragrant amine expanding and (C-H) benzeneoid and quinonoid ring bowing modes. The presence of the most noteworthy 'electronic like' bond in the scope of GOTPL, found at 1123  $\text{cm}^{-1}$ , shows that this model will have favored conductivity over GOTP. The extended conductivity in this model could be attributable to the PANI chains' long fiber-like shape.

### **RAMAN SPECTROSCOPY:**

The improvement of the D band at 1350  $\text{cm}^{-1}$  and the G band at 1595  $\text{cm}^{-1}$  in Figure is inferable from the doubly degenerate strategy for E<sub>2g</sub> equity and gets from the in plane vibration of sp<sup>2</sup> hybridized carbon particles. On account of GOT, the ID/IG extent has extended to 1.3 from 1.06 in a relative reach for GO. This clearly shows that the expansion of APQD moieties through the edges of GO sheets and their (-) stacking with fragrant rings of GO has exacerbated fundamental flimsiness in GOT. The sign for (C=C) broadening vibration at 1595  $\text{cm}^{-1}$  and protonated (C-N) expanding vibration at 1345  $\text{cm}^{-1}$  coordinates with the D and G bunches in GOTPL. The broadening vibration (C=N) of 1540  $\text{cm}^{-1}$  covers with the expanding or G band signal (C=C). Beside the other applicable GO and PANI signals, the recently referenced extensive signs are particularly significant since they suggest wide PANI chain relationship with the GO surface. It's vital that the Raman spectra of GOTP shows a model that is like that of GOTPL. The broadness

is decreased by virtue of non-covalently coupled GO/PANI for GOPL, which could show less association between GO sheets and PANI chains.

### WAXS ANALYSIS:

Figure represents the WAXS examination, which shows comparable tops to those depicted in part III. Signals comparing to resemble and opposite planes of PANI chains can be found at  $2\theta = 14.79$  (011 plane),  $19.89$  (020 plane), and  $25.81$  (200 plane) on account of GOTPL. Aside from this, signs at  $2\theta = 6.65$  and  $8.99$  highlight expanding interlayer partition of GO crystallites because of PANI chain development and collaborations. Because of the equal and opposite planes of PANI, equivalent signs for PANI chains are found at  $2\theta = 15.55$ ,  $21.33$ , and  $25.33$  for the recently referenced planes on account of GOPL. Aside from these, more keen signs should be visible at  $2\theta = 16.78$ ,  $18.34$ ,  $19.23$ , and  $23.34$ . The clarification for the creation of these signs is obscure, but the development of CSA(-) delivered similar PANI crystallinities because of poor PANI chain collaboration with the GO surface could be one chance. Be that as it may, because of the non-covalent connection of PANI chains to the GO surface, the mediocre cooperation comparative with GOTPL is not out of the ordinary.

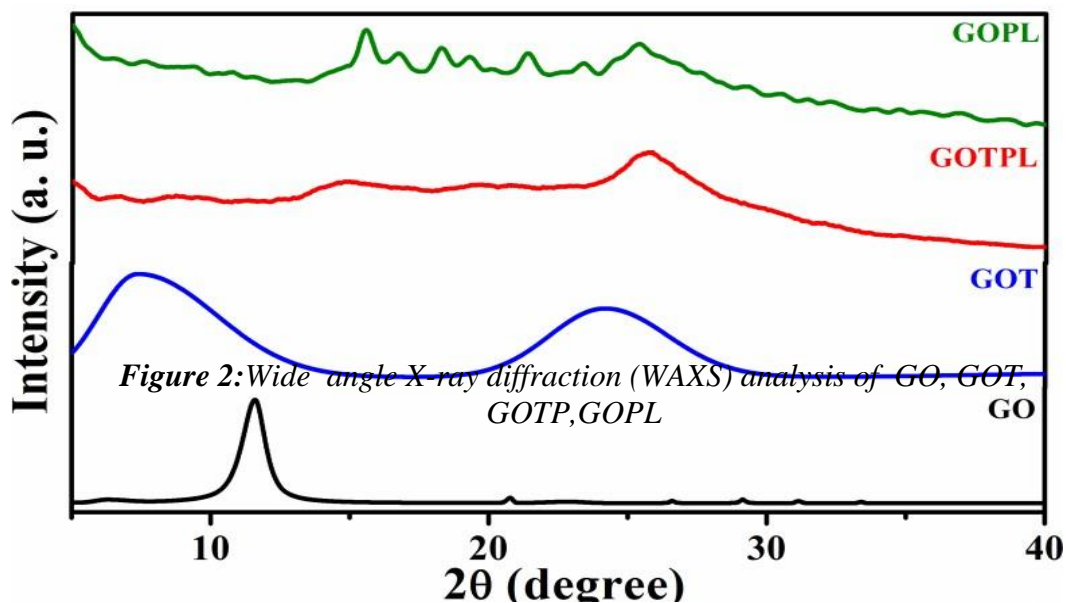


**Figure 4.3:** Wide angle X-ray diffraction (WAXS) analysis of GO, GOT, GOTP, GOPL

### CD Spectral Analysis:

The CD spectra of GOTP, GOPL, and GOTPL are displayed in Figure 4.4. Obviously, there is no sign showing achiral PANI chains in the example of GOTP. On account of GOPL, notwithstanding, dextrochirality is undeniably more uncommon. On account of GOTPL, notwithstanding, an extreme sign is found at 418 nm. The significantly quicker speed of response catalyzed by APQD moieties is connected with the enormous expansion in chirality.

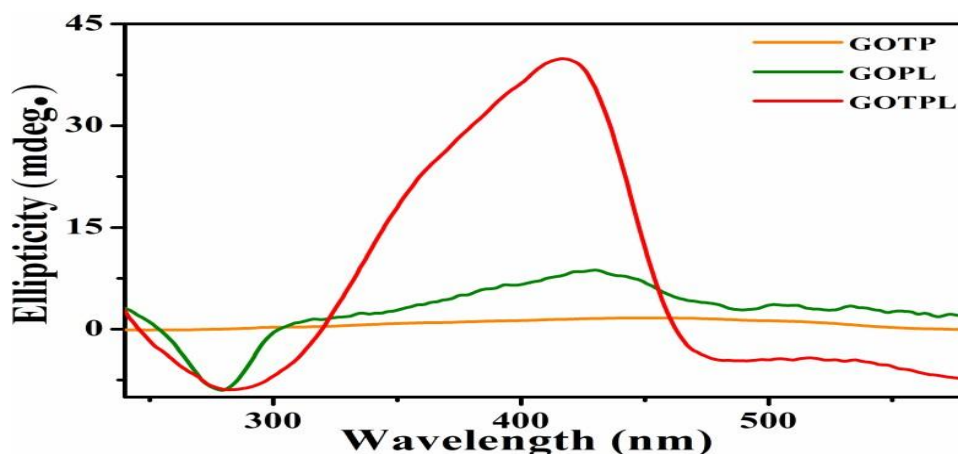


Figure :3 CD Spectra analysis of GOTP, GOPL,GOTPL

Figure depicts the enantioselective thought of this mix, which shows an almost indistinguishable portrayal like sign by virtue of GOTPL and GOTPD tests when aniline polymerization is completed within the sight of L-HCSA or D-HCSA, separately.

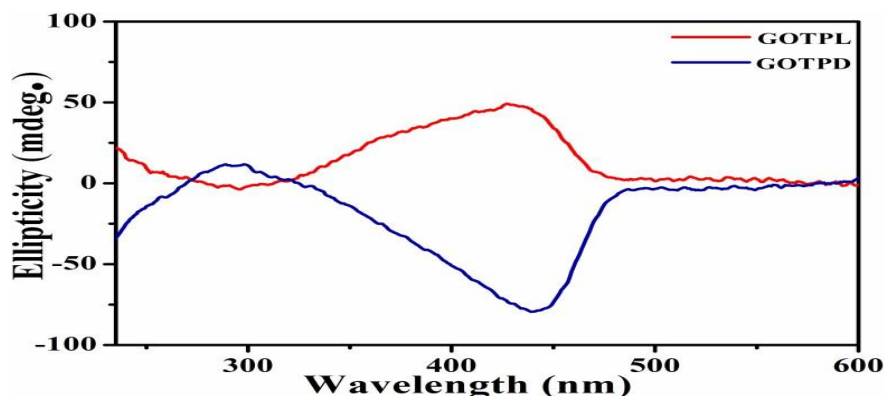
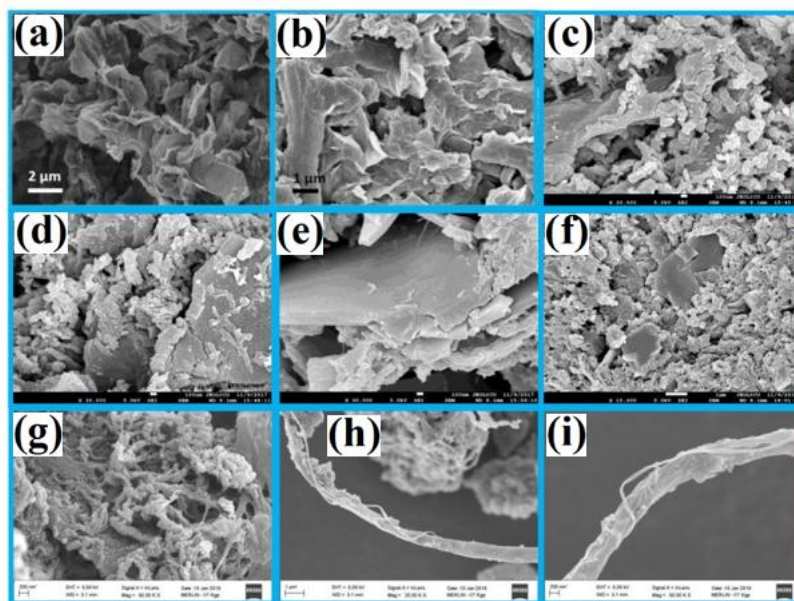


Figure:4CD Spectral analysis of GOTPL,GOTPD

**FESEM Analysis:**

Figure 4 shows FESEM pictures of GO and GOT with unmistakably tremendous GO sheets with micrometre size ranges, yet on a very basic level more unassuming GOT sheets. Nano composed PANI spaces covering the GO surface, as well as comparably more noteworthy PANI chambers or arbitrarily coupled PANI filaments, might be seen in GOTP GOPL, then again, obviously uncovers level GO surfaces with no PANI chain development, for example withdrawn GO sheets and PANI chains. Another view, displayed in Figure 4.6f, shows arbitrarily associated PANI strands and the discrete appearance of non-PANI joined GO sheets. Be that as it may, no felicity of PANI filaments should be visible in any of the photographs. This could be on the grounds that to the low level of chirality made during the response, as found in CD spectra. On account of GOTPL, be that as it may, Figure 4.6g shows GO surface associated nanostructured PANI chains as well as rather enormous helical PANI chains. Figure 4 shows PANI fiber packs with obviously clear felicity.



**Figure :5 FESEM images of (a) GO, (b) GOT, (c, d) GOTP, (e, f)GOPLand (g,h, i)GOTPL**

### HRTEM Analysis :

Figure 5 shows HRTEM pictures of GO and GOT, with the haziness in the large GO sheet owing to the - stacked GO sheets. On account of GOT, in any case, clear sheet pictures are acquired because of significantly more grounded shedding of GO sheets. outlines the improvement of more splendid PANI spaces over less light GO sheets in an achiral GO-g-PANI nanocomposites (GOTP) HRTEM picture. Figure 5 shows helical chains in GOTPL, a chiral nanocomposite, with an amplified view in the inset of the figure 5.

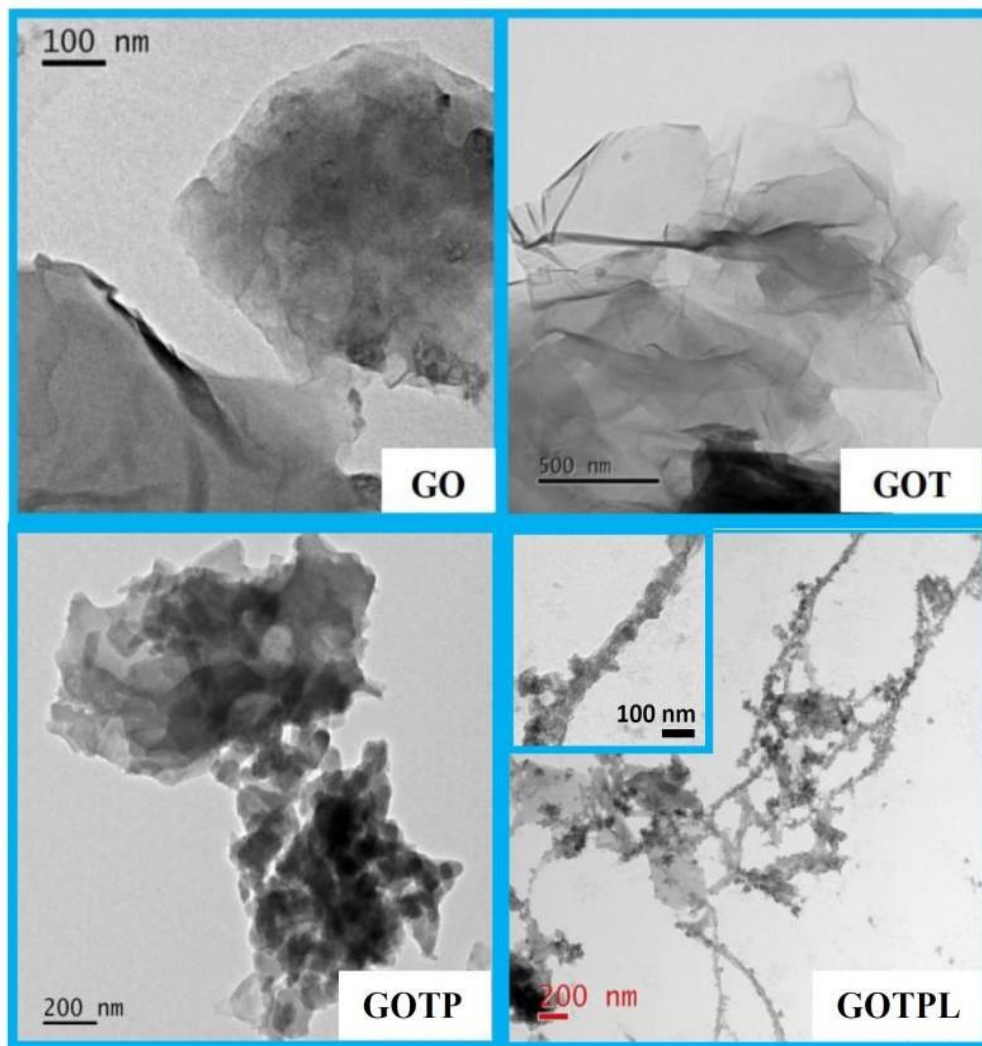


**Figure:6 HRTEM image of GO, GOT, GOTP andGOTPL**

Due to the CD audit, felicity acknowledgment is found in GOTPL tests, but the degree of chirality is impressively lower in GOPL tests. The end is moreover maintained by the morphological assessment.

**ELECTROCHEMICAL STUDY**

PANI filaments with helical strands are projected to have a bigger surface region. Accordingly, the covalently fortified chiral nano composites are supposed to have better electrochemical attributes. Figure shows the overlay of GOPL, GOTPL, and GOTP CV follows. The presence of a semi rectangular shape in the CV bend proposes the activity of electrochemical twofold layer capacitance (EDLC). Moreover, a couple of tops at 0.19V (oxidation) and a wide sets of tops close 0.42V (oxidation) might be found on account of GOPL. The reversible redox progress is liable for the primary sets of pinnacles.

between PANI's leucoemeraldine and pernigraniline states For the situation of GOTPL and GOTP, a comparable sets of pinnacles can likewise be seen. Notwithstanding the redox tops referenced over, one more sets of pinnacles might be seen at 0.72V. (for GOTPL and GOTP)

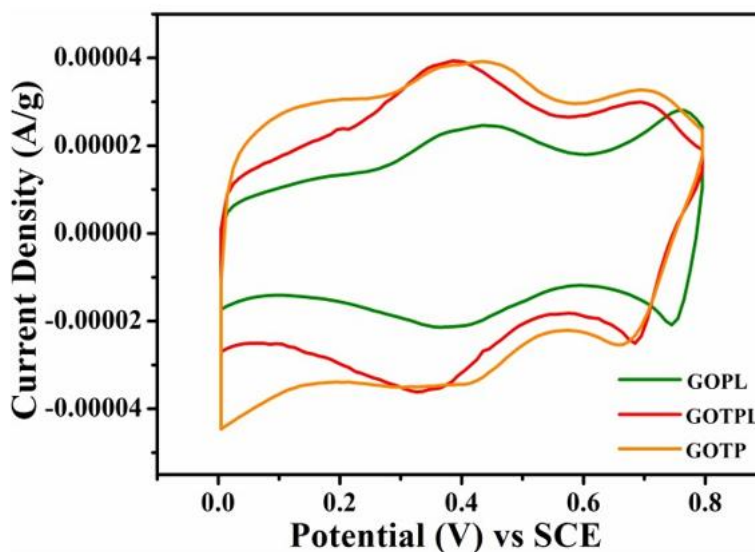


**Figure :7 CV curves of GOTP,GOPLand GOTPL**



On account of GOPL, it's 0.77V. The ortho connected aniline rings found in PANI chains are in all probability the wellspring of these pinnacles. Superposition of the redox changes of oxygenous functionalities present in a hurry surface and the emaralidine to pernigraniline progress of PANI chains could make sense of the significant broadness of redox tops close 0.42V (oxidation). While contrasting GOTPL with GOPL, the region under the pinnacle is displayed to decisively rise. This demonstrates that GOTPL has a higher explicit capacitance esteem, likely on the grounds that helical PANI chains have a bigger surface region than GOPL's haphazardly associated PANI filaments with a lower level of felicity. GOTP, then again, has a little bigger sign region under the CV bend than GOTPL. This is because of the making of nanostructured PANI chains, as seen in FESEM pictures. Nano organized anode materials have been displayed to work on unambiguous capacitance.

#### **CONCLUSION:**

It is spread out that a covalently joined GO-g-PANI chiral nano composite with chiral PANI chains impelled by optically pure HCSA is fruitful. The arrangement of helical PANI chains is spread out using CD and morphological assessment using FESEM and HRTEM. PANI chain beginning from APQD moieties related with the GO surface not simply directs there of psyche of the PANI chains, yet also prompts an amazingly more critical degree of chirality. The new designed strategy has been demonstrated to be prepared for making enantioselective GO-g-PANI nano composites created by L-HCSA or D-HCSA. Nevertheless, by virtue of non covalently attached nanocomposite (GOPL), where the improvement of PANI chains isn't progressed by APQD moieties, the degree of chiral acknowledgment is significantly lower. Finally, to the extent that energy stotage as a supercapacitor cathode, covalently built up helical PANI chains from the GO surface have a huge effect. The better surface district of the chiral nano composite and the synergistic effect of the covalently built up GO and PANI parts are responsible for the unfathomably further developed energy limit. Regardless, the energy storing property of achral yet covalently related GO-g-PANI (GOTP) nano composite has been represented to be to some degree better, possibly due to nano coordinating of PANI regions.



## REFERENCES

1. Hwang, G. L., Shieh, Y. T., & Hwang, K. C. (2019). Efficient load transfer to polymer-grafted multiwalled carbon nanotubes in polymer composites. *Advanced Functional Materials*, 14(5), 487-491.
2. Baskaran, D., Mays, J. W., & Bratcher, M. S. (2020). Polymer-grafted multiwalled carbon nanotubes through surface-initiated polymerization. *Angewandte Chemie International Edition*, 43(16), 2138-2142.
3. Viswanathan, G., Chakrapani, N., Yang, H., Wei, B., Chung, H., Cho, K., ...&Ajayan, P. M. (2003). Single-step in situ synthesis of polymer-grafted single-wall nanotube composites. *Journal of the American Chemical Society*, 125(31), 9258-9259.
4. Tsubokawa, N. (2015). Preparation and properties of polymer-grafted carbon nanotubes and nanofibers. *Polymer Journal*, 37(9), 637-655.
5. Gao, C., Jin, Y. Z., Kong, H., Whitby, R. L., Acquah, S. F., Chen, G. Y., ... & Walton, D. R. (2015). Polyurea-functionalized multiwalled carbon nanotubes: synthesis, morphology, and Raman spectroscopy. *The Journal of Physical Chemistry B*, 109(24), 11925-11932.
6. Kong, H., Luo, P., Gao, C., & Yan, D. (2015). Polyelectrolyte-functionalized multiwalled carbon nanotubes: preparation, characterization and layer-by-layer self-assembly. *Polymer*, 46(8), 2472-2485.
7. Wang, Y. P., Pei, X. W., He, X. Y., & Yuan, K. (2005). Synthesis of well-defined, polymer-grafted silica nanoparticles via reverse ATRP. *European polymer journal*, 41(6), 1326-1332.
8. Xie, X. L., Mai, Y. W., & Zhou, X. P. (2005). Dispersion and alignment of carbon nanotubes in polymer matrix: a review. *Materials science and engineering: R: Reports*, 49(4), 89-112.
9. Lou, X., Detrembleur, C., Sciannamea, V., Pagnouille, C., & Jérôme, R. (2004). Grafting of alkoxyamine end-capped (co) polymers onto multi-walled carbon nanotubes. *Polymer*, 45(18), 6097-6102.
10. Viswanathan, G. (2014). *Polymer grafted single-walled carbon nanotube composites*. Rensselaer Polytechnic Institute.